

Exploring PVFM-Based Janus Membrane-Supporting Gel Polymer Electrolyte for Highly Durable Li–O₂ Batteries

Nan Meng,[†] Fang Lian,^{*,†} Yadi Li,[†] Xiaofeng Zhao,[†] Li Zhang,[‡] Shigang Lu,[‡] and Hong Li[§]

[†]School of Materials Science and Engineering, University of Science and Technology Beijing, Beijing 100083, China

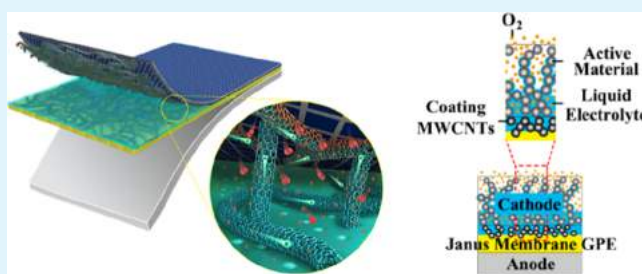
[‡]China Automotive Battery Research Institute Co. Ltd., Beijing 100088, China

[§]Beijing National Laboratory for Condensed Matter Physics, Institute of Physics, Chinese Academy of Sciences, Beijing 100190, China

Supporting Information

ABSTRACT: Electrolyte is the key to constructing the ionic transport paths and O₂ gas diffusion routes in the cathode as well as maintaining the electrode interfacial stability in view of the complex chemistry of Li–O₂ batteries. A novel poly(vinyl formal) (PVFM)-based Janus membrane, which is prepared via coating multiwalled carbon nanotubes (MWCNTs) on the porous side of the cross-linked PVFM membrane, has been proposed herein to achieve membrane-supporting gel polymer electrolyte (GPE) for Li–O₂ batteries. Within Li–O₂ batteries, the dense side of PVFM-based Janus membrane demonstrates a good compatibility with lithium metal anode, while the other side with MWCNTs coating reserves much more solvent on the surface, assisting the cathode to form enlarged electrolyte-wetted interface. Moreover, the comparative studies indicate that PVFM-based Janus membrane also can provide a conductive pathway, modulate the morphology of the discharge products, and produce accommodation space for the products. So, the Li–O₂ batteries containing PVFM-based Janus membrane-supporting GPE not only demonstrate significantly improved discharge capacity and cycling stability, i.e., 150 times at 1000 mAh g⁻¹ capacity limitation, but also a narrow voltage gap of 0.90 V and an excellent rate performance up to 1000 mA g⁻¹.

KEYWORDS: lithium–O₂ battery, polymer electrolyte, membrane, electrochemical reversibility, electrode compatibility



1. INTRODUCTION

Li–O₂ batteries employ oxygen as active material and lithium metal as anode, so their energy density is not restricted by the cathode capacity and easily reach 500 Wh kg⁻¹,^{1,2} realizing a driving range of 800 km per charge of the electric vehicles.^{3,4} Within an aprotic solvent-based Li–O₂ battery, the fundamental discharge reactions based on the solution and surface chemistries are considered to be O₂ + e⁻ + Li⁺ → LiO₂ and 2LiO₂ → Li₂O₂ + O₂,⁵ where the dynamics of oxygen reduction reaction (ORR) and oxygen evolution reaction (OER) depend on the triple-phase boundary simultaneously containing Li⁺- and e⁻-transport paths and O₂ gas diffusion routes. It is noteworthy that submergence of the cathode in the electrolyte, liquid or gelatinous, leads to the blocking of O₂ diffusion and large polarization of the electrochemical reaction based solely on the dissolved oxygen gas in the electrolyte. Additionally, the commercial carbonate-based electrolyte has been proven to decompose during cycle under the attack of the superoxide radical (O₂^{•-}).⁶ In the meantime, conventional liquid electrolytes are volatile causing rapid exhaustion and safety concerns in an open Li–O₂ battery system. In view of the above issues of the electrolyte for Li–O₂ batteries, gel polymer electrolytes (GPEs) based on poly(ethylene oxide),⁷

poly(methyl methacrylate),⁸ poly(vinylidene fluoride),⁹ its hexafluoropropylene copolymers¹⁰ and so on were extensively studied to improve the durability and safety of Li–O₂ batteries. Moreover, the mechanical and electrochemical properties of GPE can be further enhanced by combining with glass fiber mat, nonwoven fabrics, and inorganic particles,^{11–14} and also GPE is reported to construct the protection layer for lithium anode from corrosion and dendrites.^{15,16} What is more, the flexibility of GPE Li–O₂ batteries makes it a good prospect of application in wearable electronic devices.^{17–19} Among various GPEs, membrane-supporting GPE should be a good choice because the polymer chains swell in the aprotic electrolyte, which contributes to lowering vapor pressure and increasing stability of the electrolyte system. Furthermore, it can assist to form the thin electrolyte-wetted layer on the cathode, which allows an increased depth of diffusion of O₂ gas.²⁰ But their application has suffered from a lack of active reaction zone due to a limited electrolyte–cathode interface for the thick cathode.

Received: April 3, 2018

Accepted: June 13, 2018

Published: June 13, 2018

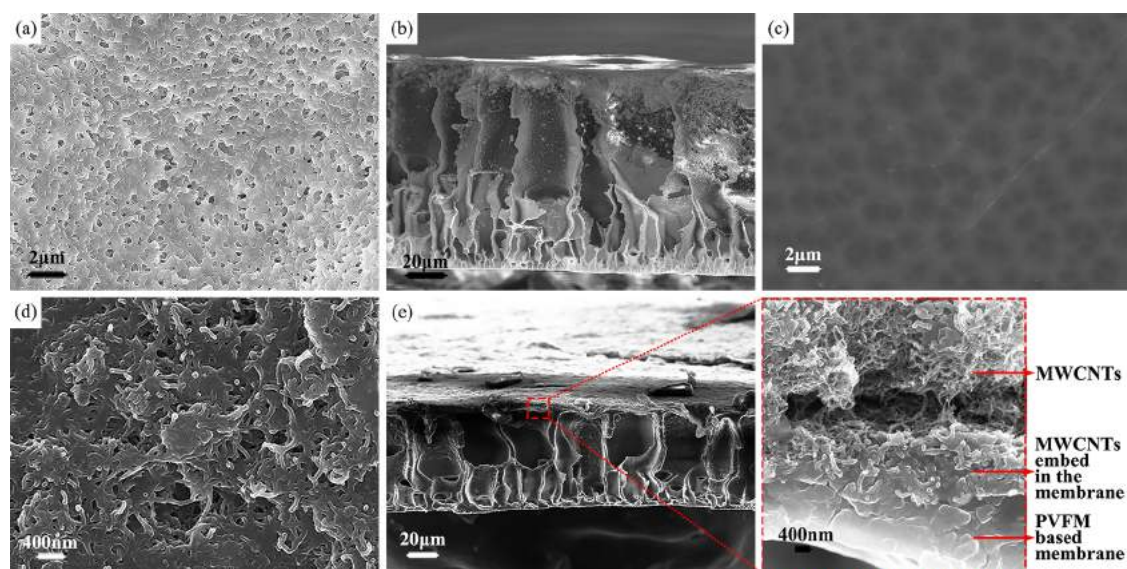


Figure 1. Scanning electron microscopy (SEM) image of the PVFM-based membrane: (a) porous side; (b) cross section; and (c) dense side. SEM image of the Janus membrane: (d) MWCNTs-coated side and (e) cross section.

In our previous study, chemical cross-linked poly(vinyl formal) (PVFM) has been developed to be a suitable polymer matrix of gel electrolyte and single-ion solid electrolyte for lithium-ion batteries because of its low glass-transition temperature (T_g), high delocalization of lithium ions, unique film-forming properties, and flexibility in modification.^{21,22} Moreover, PVFM-based membrane-supporting GPE was one of the attractive species, possessing a high liquid uptake, a good conductivity of 10^{-3} S cm^{-1} , and a wide electrochemical window up to 5.0 V.²³ Although the application of PVFM-based membrane-supporting GPE in Li–O₂ batteries solves the rapid exhaustion of nonaqueous liquid electrolytes and has access to high durability of Li–O₂ batteries with an open system, the stability on the surface of lithium metal anode and against attack by the superoxide radical (O₂^{•−}) is still questionable. Especially, expanding the cathode/electrolyte interface becomes much more crucial of the application of GPE in Li–O₂ batteries.

In this contribution, a novel PVFM-based Janus membrane has been proposed as the gel polymer electrolyte supporter, consisting of one dense side and the other porous side with multiwalled carbon nanotubes (MWCNTs) coating. Moreover, the solvent for GPE is considered herein to improve their stability, ionic conductivity, and anode compatibility for Li–O₂ batteries. In addition to inheriting the advantages of membrane-supporting GPE, the PVFM-based Janus membrane is expected to assist the cathode to reconstruct the interfacial chemistry, which provides a solution to improve the cycle life and energy density of the polymer electrolyte Li–O₂ batteries.

2. EXPERIMENTAL SECTION

2.1. Preparation of the PVFM-Based Janus Membrane. The 4,4'-diphenylmethane diisocyanate (Alfa Aesar) cross-linked PVFM (Sigma-Aldrich) membrane with a thickness of about 100 μm was prepared by the phase inversion technique.²³ MWCNTs (Cnano Technology) were dispersed in the mixture of *N*-methyl pyrrolidone (NMP, Sinopharm) and deionized water with PVFM as binder. The MWCNTs slurry was coated on the porous side of the PVFM-based membrane using an airbrush, and then the membrane was dried at 100 °C for 1 h. The coating and drying processes were repeated five times, and finally, the membrane with MWCNTs coating layer was

dried under vacuum at 100 °C for 24 h to achieve PVFM-based Janus membrane.

2.2. Characterization of the Membrane. The surface morphology of the PVFM-based membrane and the Janus membrane was observed using a field emission scanning electron microscope (FESEM) (SUPRA55, Carl Zeiss, Germany). Wettability was tested on a contact angle meter (JC2000C1, Zhongchen, China); in the test, a drop of the electrolyte composed of 1.1 mol L^{−1} lithium bis-(trifluoromethanesulfonyl)imide (LiTFSI) in the mixed solvents of dimethyl sulfoxide (DMSO) and tetraethylene glycol dimethyl ether (TEGDME) with a volume ratio of 8:2 was dripped on the MWCNTs coating side of the Janus membrane, and the contact angle was fitted from the photo taken after 30 s.

2.3. Matching with Electrolyte and Its Characterization. The PVFM-based membranes and the Janus membranes were punched into disks of 16 mm in diameter, dropping 200 μL of the liquid electrolyte to the membranes in the argon-filled glove box, where the content of water and oxygen was less than 0.5 ppm. The membrane absorbed the liquid electrolyte and swelled the polymer chains to form GPE. In view of the good stability of lithium bis-(trifluoromethanesulfonyl)imide (LiTFSI, Aladdin) and the sulfone/ether solvents in the Li–O₂ (air) batteries as reported,²⁴ LiTFSI dissolved in the solvent of dimethyl sulfoxide (DMSO, J&K) and/or tetraethylene glycol dimethyl ether (TEGDME, Aladdin) was chosen to form the membrane-supporting GPE for Li–O₂ batteries. Furthermore, the liquid electrolyte composed of 1.1 mol L^{−1} LiTFSI and the mixed solvents of DMSO and TEGDME in a volume ratio of 8:2 was determined with the ionic conductivity as the primary strategies in the mass triangle model calculation, which was shown as Figure S1 and Table S1 in the Supporting Information.

The conductivity of the GPE was measured by alternating current (ac) impedance spectroscopy (VersaSTAT 3, Princeton Applied Research), and the electrochemical stability of the electrolyte was measured by linear scan voltammetry at 25 °C. Thermal stability of the electrolytes was investigated by thermogravimetric analysis (TGA, Q2000, TA Instruments) from room temperature to 600 °C at a heating rate of 10 °C min^{−1} in argon atmosphere. The compatibility of GPE with lithium metal in oxygen atmosphere was investigated by the ac impedance spectroscopy using Li/the PVFM-based Janus membrane-supporting GPE/stainless steel mesh cells with a potential amplitude of 5 mV from 100 to 0.01 kHz and Li stripping–deposition measurements (CT2001A, Wuhan Land Electronic Co. Ltd., China) using the symmetrical Li/the PVFM-based Janus membrane-

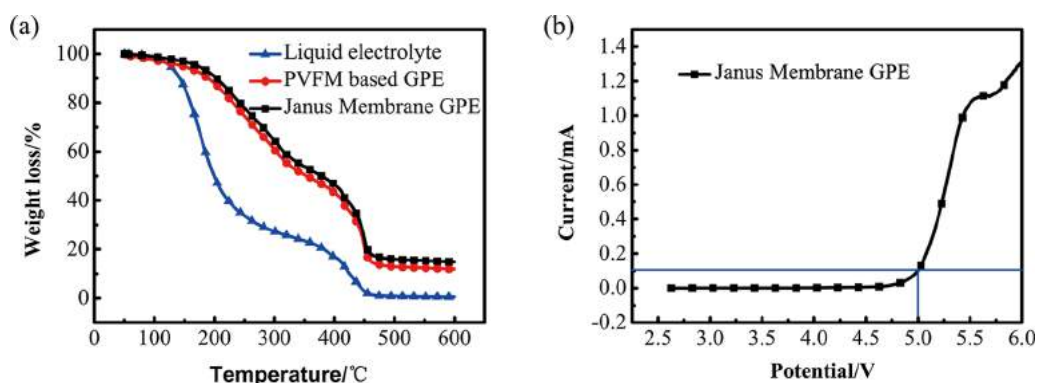


Figure 2. a) TGA of the liquid electrolyte, the PVFM-based membrane, and the Janus membrane-supporting GPE. (b) The linear sweep voltammetry curves of the Janus membrane-supporting GPE.

supporting GPE/Li cell at 0.1 mA cm^{-2} per process and a stripping–deposition time of 30 min.

2.4. Assembly and Test of Li–O₂ Battery. A slice of commercial carbon paper (NOSN05, CeTech, China) with MWCNTs coating was adopted herein as the cathode. The coin cells were assembled by sandwiching the PVFM-based Janus membrane between lithium metal anode and cathode as illustrated in Figure S2, in detail with the dense side facing Li metal and the porous side with MWCNTs coating facing the cathode. Then, 200 μL of the liquid electrolyte composed of 1.1 mol L^{-1} LiTFSI and the mixed solvents of DMSO and TEGDME in a volume ratio of 8:2 was dropped into the cells, which were kept in the argon-filled glove box for 8 h before the electrochemical test. To further evaluate the function and applicability of the Janus membrane, polymer lithium–oxygen batteries with $\delta\text{-MnO}_2\text{@CNTs}$ as the cathode material were also assembled by the aforementioned method. Charge-transfer resistance of the Li–O₂ batteries with GPE was analyzed by impedance tests before cycling and after 1st, 5th, 10th, and 15th cycle with a potential amplitude of 5 mV from 100 to 0.01 kHz. Galvanostatic circulation tests were conducted by a battery tester (CT-3008-164, NEWARE, China) with a limitation of capacity or in a voltage window of 2.0–4.5 V (vs Li/Li⁺). The discharge products collected from disassembled batteries were investigated by the FESEM, Fourier transform infrared (FTIR) spectroscopy (FT-IR670, NEXUS), and X-ray diffraction (XRD, TTRIII, Rigaku, Japan).

3. RESULTS AND DISCUSSION

The morphology of the PVFM-based membrane and the PVFM-based Janus membrane is demonstrated in Figure 1. PVFM-based membrane was prepared via the phase inversion process starting from the region of the poor phase nucleation metastable gap in the ternary-phase diagram.²³ The obtained PVFM membrane demonstrates an asymmetric structure with a porous layer on the one side, a dense layer on the other side, and a finger-like porous profile, as shown in Figure 1a–c. MWCNTs are homogeneously coated on the porous side of the PVFM-based Janus membrane with a thickness of 2–4 μm and carbon loadings of 0.2–0.4 mg cm^{-2} . In more detail, most of the MWCNTs disperse on the surface of the membrane, and a small amount of MWCNTs embed in the membrane, which is contributed to the NMP-induced slight swelling of PVFM membrane in the coating process. But the original architecture including the finger-like porous cross section is retained well in the membrane. Moreover, in comparison with the PVFM-based membrane, the Janus membrane exhibits the improved mechanical strength, as shown in Figure S3. MWCNTs bonded on the porous side of the membrane refill part of

the surface pore and strengthen the polymer chain through hydrogen bonding or van der Waals force.²⁵

Considering the chemical stability, ionic conductivity, and electrode compatibility of the electrolyte system for Li–O₂ batteries, LiTFSI-based electrolytes were chosen to match the Janus membranes, and different solvent-containing systems^{26–31} were compared as shown in Table S2. DMSO is commonly used in Li–O₂ battery^{24,32} owing to its high donor number, low volatility and viscosity, good oxygen diffusion ability, and high conductivity. Furthermore, solvent can be cross-linked with the polymer matrix of GPE to further improve its stability on the surface of lithium metal as previously reported.³³ In our study, the mixing of DMSO/TEGDME solvents is accessible to the high ionic conductivity and the appropriate swelling of the PVFM-based membrane. So, the electrolyte matching with the Janus membrane including the ratio of DMSO/TEGDME and the concentration of LiTFSI was optimized by the mass triangle model calculation with ionic conductivity as the primary strategy.³⁴ As a result, a formula of 1.1 mol L^{-1} LiTFSI dissolved in the mixed solvents of DMSO and TEGDME in a volume ratio of 8:2 is chosen herein, and the ionic conductivity of the Janus membrane-supporting GPE reaches $1.01 \times 10^{-3} \text{ S cm}^{-1}$. The PVFM-based membrane and the Janus membrane were soaked in the liquid electrolyte for 5 h. Their average absorption rate reaches 475.8 and 439.7%, respectively, which is much higher than that of glass fiber separator 187.8% (GF/D, Whatman). Moreover, the mass loss of the electrolyte in 480 h is less than 15% when completely exposed to the air. By contrast, 30–60% electrolyte (depending on the liquid electrolyte species) evaporates without PVFM-based membrane or the Janus membrane as supporters. The results indicate that membrane-supporting gel polymer electrolyte shows significantly improved electrolyte retention.

Additionally, the thermal stability of the Janus membrane-supporting GPE was analyzed by TGA measurement at a heating rate of $10 \text{ }^\circ\text{C min}^{-1}$ in argon atmosphere and compared with that of PVFM-based membrane-supporting GPE and liquid electrolyte in Figure 2a. It can be observed that liquid electrolyte and GPE begin significant weight loss at 142.24 and 198.74 $^\circ\text{C}$, respectively. At around 150 $^\circ\text{C}$, the liquid electrolyte shows a weight loss of 13.81 wt %, whereas PVFM-based membrane-supporting GPE exhibits a weight loss of 5.18 wt % and the Janus membrane-supporting GPE 3.14 wt %. At around 200 $^\circ\text{C}$, the thermal stability of the Janus membrane-supporting GPE is much more outstanding with a

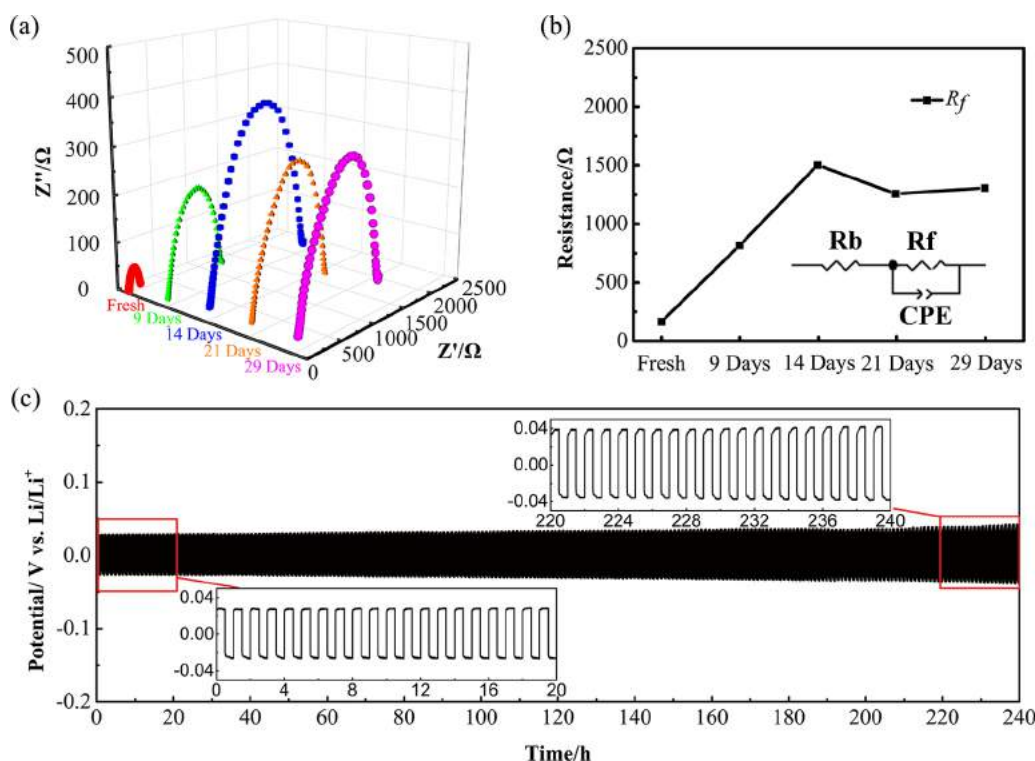


Figure 3. Compatibility of the Janus membrane-supporting GPE with lithium metal anode. Evolution of the resistance value in a Li/the Janus membrane GPE/O₂ cell upon storage time: (a) the Nyquist plots in oxygen atmosphere and (b) equivalent-circuit parameters of the Janus membrane-supporting GPE with lithium metal anode in O₂. (c) Voltage–time curves of the Li stripping–deposition measurements using the symmetrical Li/the Janus membrane GPE/Li cell at 0.1 mA cm⁻² per process and a deposition/stripping time of 30 min.

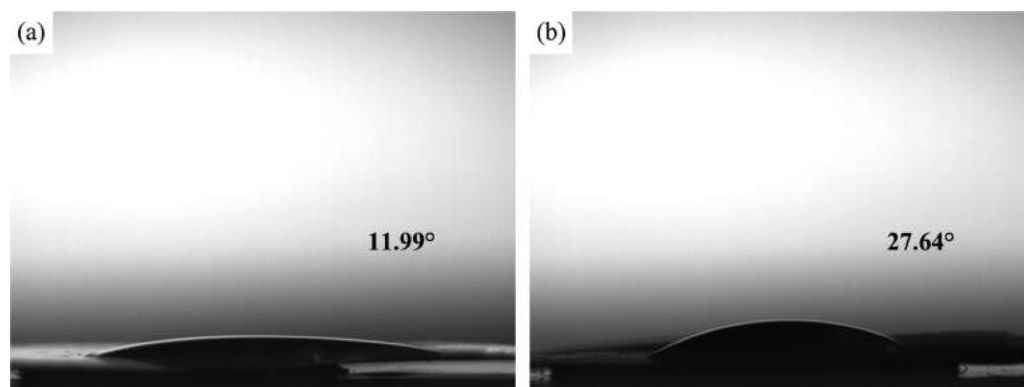


Figure 4. Contact angle of the liquid electrolyte on (a) the porous side of PVFM-based membrane and (b) the MWCNTs-coated side of the Janus membrane.

weight loss of 9.31 wt % than the PVFM-based membrane-supporting GPE with 12.10 wt % and the liquid electrolyte with 50.39 wt %. The thermal stability of the electrolyte is improved with the application of PVFM matrix, which is attributed to that the three-dimensional polymer network formed in GPE, and the MWCNTs coating layer further blocks the liquid components. Moreover, the oxidative decomposition behavior of the Janus membrane-supporting GPE was also investigated by linear sweep voltammetry (LSV). As shown in Figure 2b, no distinct oxidation peaks are observed up to 5.0 V (vs Li/Li⁺) for the Janus membrane-supporting GPE. Therefore, the Janus membrane-containing DMSO/TEGDME-based electrolyte shows a high durability, which is a promising candidate of the electrolyte for Li–O₂ batteries.

The compatibility of the Janus membrane-supporting GPE with lithium metal anode in O₂ was investigated by ac impedance spectroscopy at open-circuit potential. A semiopen cell with a construction of Li/the Janus membrane electrolyte/stainless steel mesh was exposed to an oxygen atmosphere and tested around every 7 days. Typical Nyquist plot for the semiopen cell with time is exhibited in Figure 3a. The intercepts with the real axis at high frequency are associated with the bulk resistance (R_b), and the low frequency, which controlled by the diffusion process, is related to the resistance of the Li/electrolyte interface (R_f).^{8,35} The width of the semicircles corresponding to R_f presents conspicuous increase when the cell was exposed to oxygen and reaches the maximum value of 1500 Ω after 14 days. Gradually, the impedance was time insensitive around 1250 Ω. This tendency

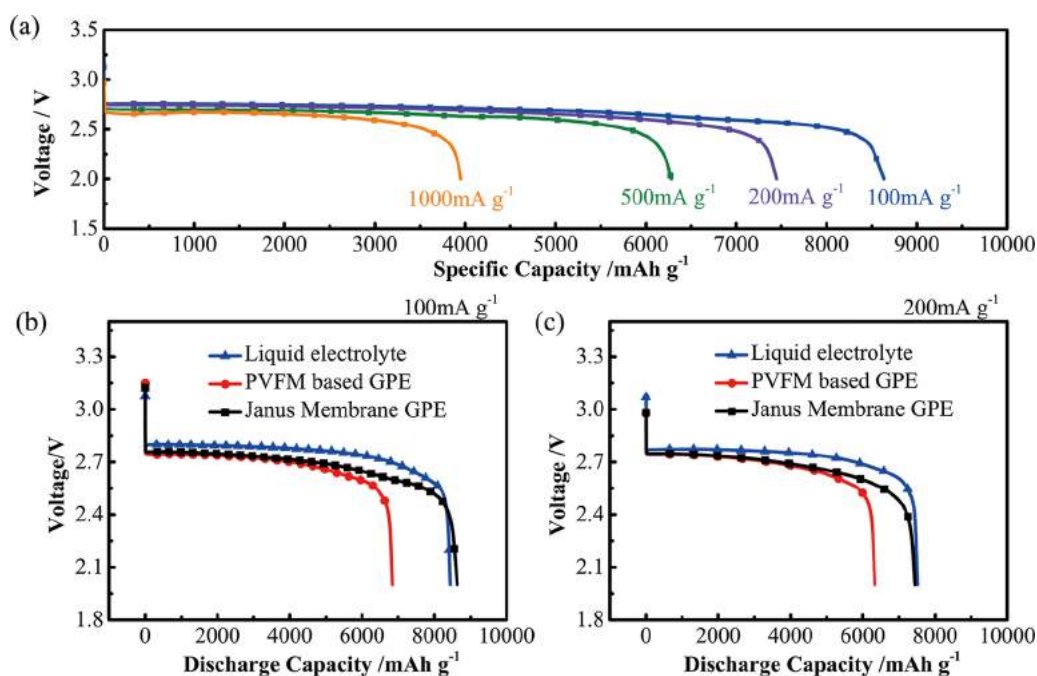


Figure 5. Galvanostatic discharge profiles of Li–O₂ battery: (a) galvanostatic discharge profiles of Li–O₂ battery with the Janus membrane-supporting GPE above 2.0 V. Galvanostatic discharge profiles of Li–O₂ battery above 2.0 V at a current density of (b) 100 mA g⁻¹ and (c) 200 mA g⁻¹.

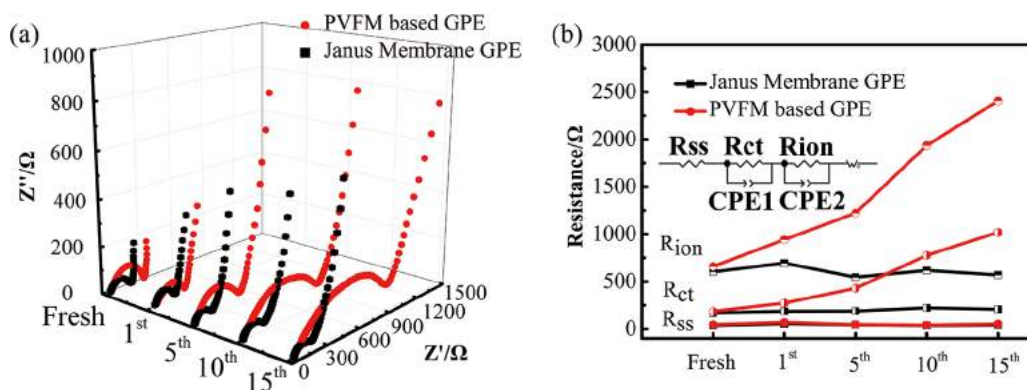


Figure 6. Impedance analysis of the Li–O₂ batteries with GPE: (a) electrochemical impedance spectroscopy plots of Li–O₂ batteries before and after cycling and (b) equivalent-circuit parameters upon various cycles with different GPE.

appears on account of the formation of a solid electrolyte interphase film at the lithium surface due to partial reaction with the electrolyte and its subsequent consolidation and stabilization,^{36,37} which indicates that the Janus membrane-supporting GPE could stabilize lithium metal anode interface from oxygen attack. Moreover, stability of Li stripping–deposition measurement of the Janus membrane-supporting GPE was analyzed by galvanostatic cycling of symmetric lithium metal cells. The corresponding voltage–time curves in Figure 3c present that the polarization value keeps low within 0.0279 V, only slightly increases to about 0.0409 V after 240 h of continuous cycling without cell failure. The stable interface resistance of the Janus membrane-supporting GPE toward lithium metal anode³⁸ and the small polarization of the symmetric lithium metal cells^{39,40} demonstrate a good compatibility of the Janus membrane-supporting GPE to the lithium metal anode in O₂ atmosphere.

The wettability of the liquid electrolyte on PVFM-based membrane and the Janus membrane was analyzed as shown in

Figure 4. The contact angle of the liquid electrolyte on the porous side PVFM-based membrane (11.99°) is much smaller than that of the MWCNTs-coated side of the Janus membrane (27.64°) in 30 s after the liquid electrolyte dripped on the membrane. The results indicate that both the PVFM-based membrane and the Janus membrane have a good wettability with the liquid electrolyte, by comparison the Janus membrane can reserve much more solvent on the surface, which is favorable to the increasing electrolyte infiltration area of the cathode.

Maximum discharge capacity of the Li–O₂ battery was evaluated at different current densities above 2.0 V. As shown in Figure 5a, a discharge capacity of 8634.4 mAh g⁻¹ is achieved in the initial discharge curve at a current density of 100 mA g⁻¹, and a plateau at 2.72 V corresponds to the formation of discharge product Li₂O₂. Even though the discharge capacity and the voltage plateau decrease with an increase of the current density, the cells with the Janus membrane-supporting GPE deliver a discharge capacity of

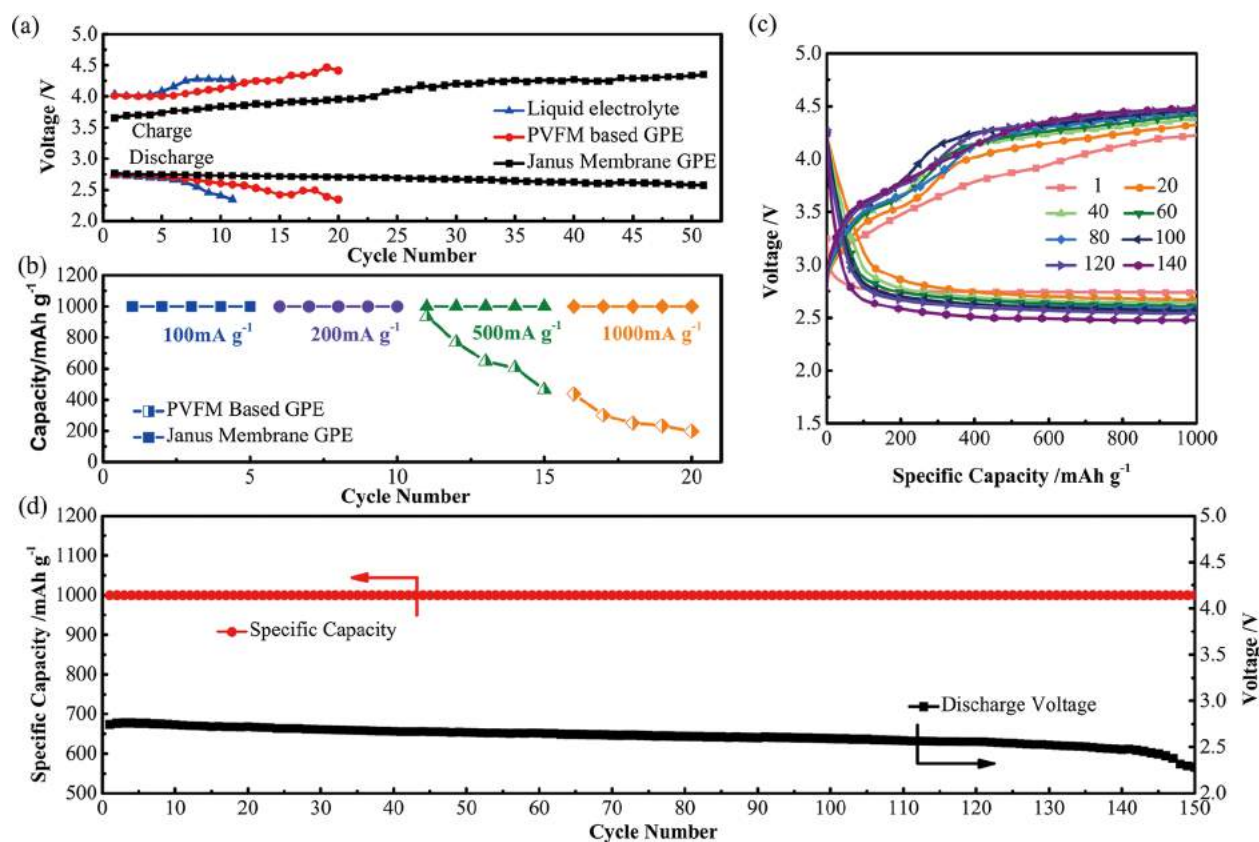


Figure 7. (a) Cycling performance of the LiTFSI-based liquid electrolyte, the PVFM-based membrane-supporting GPE, and the Janus membrane-supporting GPE at 200 mA g⁻¹ with capacity limited to 1000 mAh g⁻¹. (b) Rate performances of the PVFM-based membrane-supporting GPE and the Janus membrane-supporting GPE up to 1000 mA g⁻¹. (c, d) The cycle performance of the Li-O₂ battery with the Janus membrane-supporting electrolyte and δ -MnO₂@CNTs cathode at a current density of 200 mA g⁻¹ with capacity limited to 1000 mAh g⁻¹.

3951.2 mAh g⁻¹ at the current density of 1000 mA g⁻¹, indicating their excellent rate performance. In Figure 5b,c, the galvanostatic discharge profiles of the Li-O₂ batteries are compared among LiTFSI-based liquid electrolyte, PVFM membrane, and the Janus membrane-supporting GPE at a current density of 100 and 200 mA g⁻¹, respectively. The cell with the Janus membrane-supporting GPE delivers a discharge capacity little higher than or comparable to the sample with the liquid electrolyte. By contrast, the cells with PVFM-based membrane-supporting GPE deliver the obviously reduced maximum discharge capacity, which is contributed to the limited active reaction zone as the common issues reported in the polymer electrolyte Li-O₂ batteries.⁴¹⁻⁴³ The comparative study suggests that the active reaction zone is enlarged in the Janus membrane-supporting GPE Li-O₂ batteries, which might be contributed to the increasing electrolyte infiltration area of the cathode.

The impedance analysis was performed to detect the impact of the Janus membrane on the internal resistance of the Li-O₂ battery.^{44,45} Figure 6 shows electrochemical impedance spectroscopy (EIS) plots of the Li-O₂ batteries with GPE before cycling and after 1st, 5th, 10th, and 15th cycle, and the equivalent electrical circuit used to model the EIS is shown in the inset of Figure 6b. The R_{ss} (including the ionic resistance as well as the contact resistances) value increases slightly as the passivation layer forms on the electrodes and meanwhile decreases as the contact improved with circulation. Moreover, the fresh cell with the Janus membrane-supporting electrolyte shows the significantly reduced charge-transfer resistance (R_{ct})

than the cell with PVFM-based membrane-supporting GPE. Upon cycling, the acceleration of charge-transfer resistance slows down in the Janus membrane-containing Li-O₂ batteries, demonstrating the stability of reaction-involved interface during the ORR and OER process with the aid of the Janus membrane. In addition, the lithium-ion migration resistance (R_{ion}) at the cathode in the Janus membrane-supporting GPE cells increases in the first few cycles due to the cathode electrolyte interphase (CEI) layer formation on the cathode. Then, R_{ion} gradually decreases to and remains around 600 Ω in accompany with the subsequent consolidation and stabilization of the CEI layer and also the better infiltration of electrolyte with cathode. By comparison, R_{ion} at the cathode in the Janus membrane-supporting GPE cells is more stable than that with PVFM-based membrane-supporting GPE. An improved electrochemical reversibility of the Janus membrane-supporting GPE, which is also confirmed by the almost unanimous cyclic voltammetry curves in Figure S4 for the first 10 cycles,^{46,47} demonstrates that the Janus membrane helps to build a conductive pathway on the interface and especially preserve the stable three-phase boundary in the cathode upon cycling.^{48,49}

Figure 7a shows the cycling performance at 200 mA g⁻¹ with the capacity control of 1000 mAh g⁻¹ in a voltage range of 2.0–4.5 V (vs Li/Li⁺). Li-O₂ battery with LiTFSI-based liquid electrolyte operates only eight cycles and terminates with a sharp increase of overpotential up to 1.73 V. The battery with PVFM-based membrane-supporting GPE completes 19 cycles and terminates with an overpotential increase to 1.84 V. In

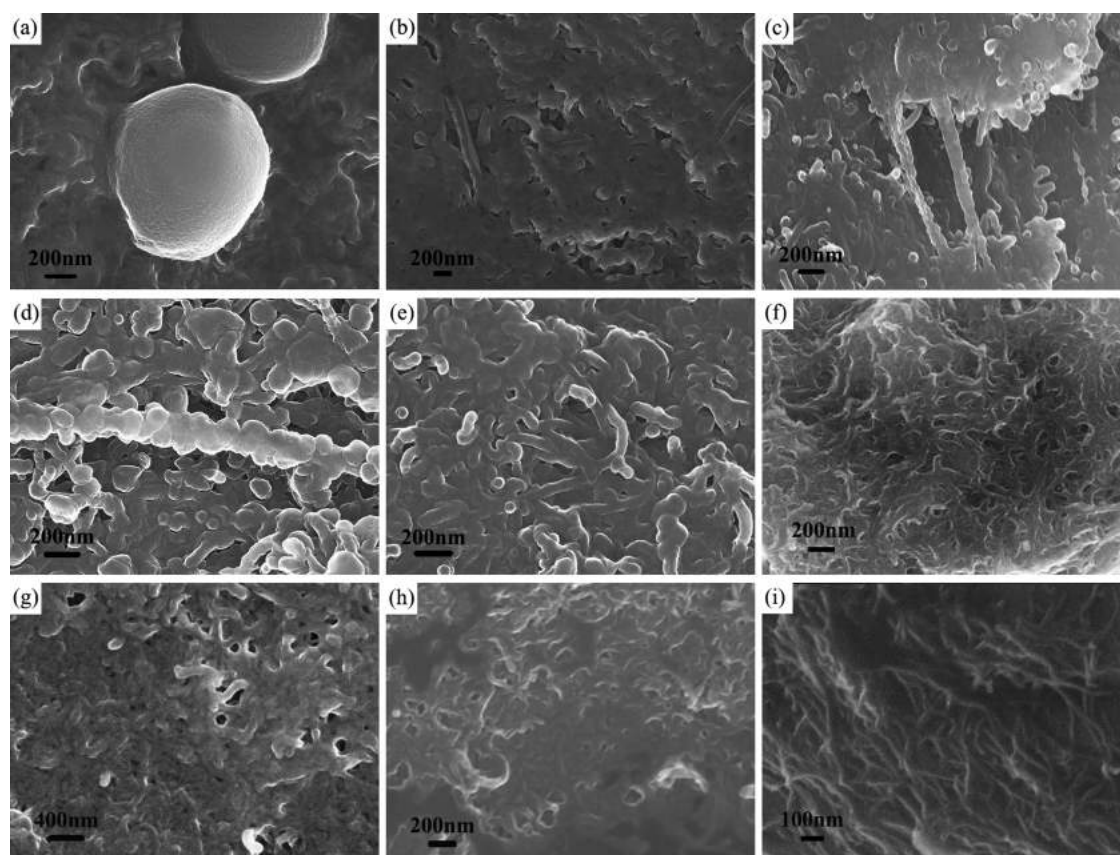


Figure 8. SEM image of the coating side of the Janus membrane: (a) after initial discharging and (b) after initial charging. SEM image of the air cathode with Janus membrane-based GPE: (c) in fresh, (d) after initial discharge, (e) after initial charge, and (f) the depth layer after 10th cycle. Morphology of the air cathode with PVFM-based GPE: (g) after initial discharge, (h) after initial charge, and (i) the depth layer after 5th cycle.

comparison with the LiTFSI-based liquid electrolyte, an improvement in electrolyte stability leads to a better cycling performance of the battery with PVFM-based membrane-supporting GPE. Furthermore, the Li–O₂ cells with the Janus membrane-supporting GPE can implement 51 cycles with a voltage gap increasing from 0.90 to 1.31 V. The rate capability of the Li–O₂ battery is shown in Figure 7b, there is no capacity fade with an increase of the current density for the cells with the Janus membrane-supporting GPE, whereas the cell with PVFM-based membrane-supporting GPE exhibits sharp capacity fade at the current density of 500 mA g⁻¹. As reported, the common current density employing in Li–O₂ batteries with GPE is about 100–200 mA g⁻¹.^{50,51} In our study, the Li–O₂ batteries with the Janus membrane-based GPE can work well even at the current density of 1000 mA g⁻¹, confirming their excellent ORR and OER kinetics. The batteries with the Janus membrane-supporting GPE achieve a greatly improved maximum discharge capacity, cycling stability, and rate capability, which is contributed by the enlarged active reaction interface, the reduced interface resistance, and the improved reversibility.

Furthermore, to clarify that the interfacial reconstruction derived from Janus membrane is the major cause for the excellent integrated properties rather than MWCNTs coating on the membrane involved in the electrochemical reaction as the major active material, the Li–O₂ cells with the Janus membrane-supporting GPE have been assembled using δ -MnO₂@CNTs as the cathode or without any cathode. As shown in Figure S5, the Li–O₂ battery without cathode

delivers a maximum discharge capacity of 517.8 mAh g⁻¹ above 2.0 V at 100 mA g⁻¹, which is only 6% of the aforementioned Li–O₂ battery capacity. So, the contribution of the coating MWCNTs as the active material can be ignored in the cells. Moreover, δ -MnO₂-coated MWCNTs with the similar microstructure of MWCNTs (as shown in Figure S6) are employed as the cathode, which is favorable to maintaining the interfacial configuration with the Janus membrane-supporting GPE in the cells. Figure 7c,d shows the voltage profiles for limiting the capacity at 1000 mAh g⁻¹ with a current density of 200 mA g⁻¹. An initial discharge plateau at 2.74 V and an initial charge plateau at 3.87 V are observed, respectively, and the voltage gap is 1.13 V in consequence. The cells with δ -MnO₂@CNTs as cathode show a significantly extended cycle life to 150 cycles, which is contributed to the better catalytic properties of MnO₂ than that of MWCNTs.^{52–54} In comparison with the previous study,^{55–58} the advancement in both GPE Li–O₂ cells depends on the interfacial modification resulting from the Janus membrane.

The Janus membrane-based GPE was further studied and compared with other electrolyte via determining the discharge product on the cathode and the coating side of the Janus membrane by FESEM, FTIR, and XRD. When the cell discharged in LiTFSI-based liquid electrolyte, the cathode is submerged in nonaqueous liquid electrolyte, leading to the blocked transportable passage of gaseous oxygen. So, the dissolved oxygen in the electrolyte becomes the sole source for the ORR process, the deposited discharge product accumulates and forms the continuous layer on the surface of the cathode as

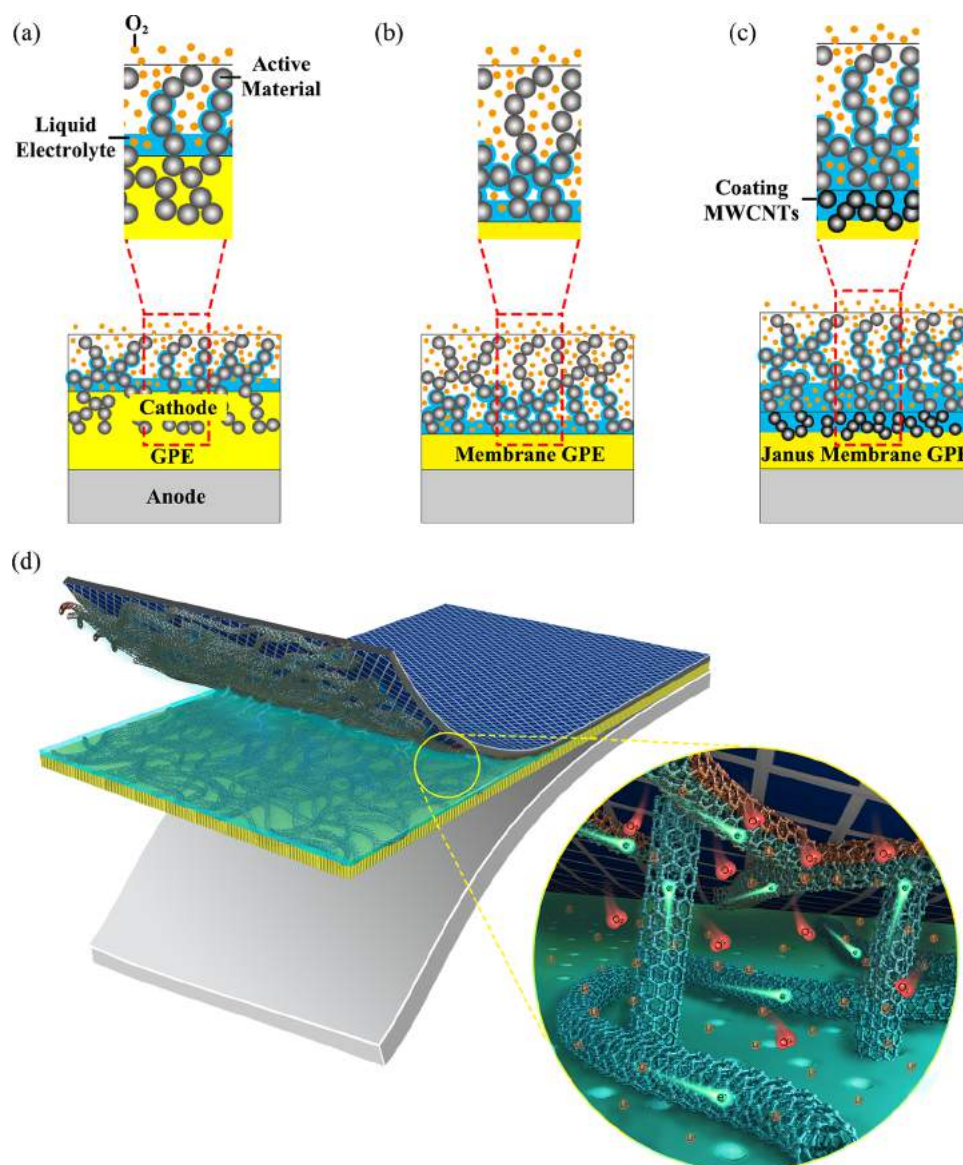


Figure 9. Schematic of the cathode infiltrating status of (a) conventional GPE, (b) membrane-supporting GPE, and (c) the Janus membrane-supporting GPE. (d) The schematic illustration of the Janus membrane-supporting gel electrolyte in the Li–O₂ batteries.

shown in Figure S7, which contributes to the significant reduction of the active ternary reaction zone. While, as shown in Figure 8g–i, the discharge product is clearly detectable as a porous layer on the surface of the cathode in the cells with PVFM-based GPE. However, after cycling, the undecomposed discharge products are accumulated and obviously observed on the surface layer of the cathode with the PVFM-based GPE, whereas MWCNTs in the depth layer show the morphology of the fresh one indicating a limited reaction area of the cathode. The partially blocked interface contributes to an increase of the charge-transfer and lithium-ion migration resistance, leading to the gradual deterioration of the cells with PVFM membrane-supporting GPE. By contrast, the discharge products with a typical spherical shape⁵⁹ in a diameter of about 100 nm appear on the carbon cathode with Janus membrane-based GPE, whereas some spherical products with a diameter of about 400 nm and a product layer are also observed on the MWCNTs coating of the Janus membrane. The FTIR and XRD results confirm that Li₂O₂ is the dominant crystalline product, as shown in Figure S8. The Janus membrane-supporting GPE

assists to construct the stable diffusion channel for oxygen, electron, and lithium ions on the cathode, which favors the nucleation process rather than the particle growth of products, leading to the formation of small discharge particles on the cathode upon discharging. The small discharge particles show the high decomposing kinetics and also facilitate the oxygen diffusion through the cathode. Moreover, the porous coating on the membrane provides the accommodation space for the discharge products. Upon charging, the small discharge particles on the cathode decompose completely, the large particles of the discharge product on the Janus membrane disappear, too. In the meantime, the XRD results of the cathode after 5th and 10th cycles in Figure S8 suggest a good reversibility of the batteries with the Janus membrane-based GPE. But the discharge products formed as the layer are still detectable on the Janus membrane. So, it is clarified that the contribution of the coating MWCNTs as the active material can be ignored due to their bad reaction kinetic in the liquid-rich domain. Meanwhile, in the presence of the Janus membrane-based GPE, the trace of electrochemical reaction

is detectable deep in the cathode, and the porous microstructure of the cathode is maintained after cycles, demonstrating the extended triple-phase boundary of ORR and OER and a significantly improved reversibility of the cathode.

Therefore, the interfacial reconstruction introduced by Janus membrane-supporting GPE could be concluded in Figure 9. The membrane-supporting GPE assists to form the thin electrolyte-wetted layer on the cathode, allowing an increased depth of diffusion of O₂ gas, which overcomes the drawbacks in the conventional GPE-containing cells. Furthermore, the MWCNTs coating reserves the much more liquid components, enlarging the electrolyte infiltration interface on the cathode as shown in Figure 9a–c. In addition, the Janus membrane-supporting GPE shows a high compatibility toward lithium anode. During the electrochemical cycling, the Janus membrane-supporting GPE contributes to the reduced interface resistance, stabilized triple-phase boundary, improved reversibility, and increased accommodation space for the discharge products, which is a reasonable candidate of the electrolyte for highly durable Li–O₂ batteries.

4. CONCLUSIONS

Lithium–oxygen batteries with extremely high theoretical energy density are a promising candidate for the next generation energy storage system. However, their practical application faces great challenges including the bad electrochemical reversibility, which is mainly attributed to the volatilization and decomposition of the electrolyte, the blocked cathode, and the limited reaction kinetics of discharge product, besides the metal lithium anode issues. In our study, a novel PVFM-based Janus membrane was prepared via coating multiwalled carbon nanotubes (MWCNTs) on the porous side of poly(vinyl formal) (PVFM)-based membrane to develop the gel polymer electrolyte (GPE) Li–O₂ batteries with advanced electrochemical reversibility. The results demonstrate that the Janus membrane-supporting GPE shows a good compatibility toward lithium anode, carbon-based and MnO₂ cathode. Furthermore, the Janus membrane-supporting GPE is responsible to extend and maintain the stable triple-phase boundary for oxygen reduction reaction (ORR) and oxygen evolution reaction (OER) and reduces the interface resistance between cathode and electrolyte. In consequence, the Li–O₂ batteries with the Janus membrane achieve a remarkable circulation of 150 cycles, a narrow voltage gap of 0.90 V, a maximal discharge capacity of 8634.4 mAh g⁻¹, and an excellent rate performance up to 1000 mA g⁻¹. The study provides an insight into the development of polymer Li–O₂ batteries with long cycle life and high-energy density.

■ ASSOCIATED CONTENT

Supporting Information

The Supporting Information is available free of charge on the ACS Publications website at DOI: 10.1021/acsami.8b05393.

Mass triangle model calculation for the conductivity of the electrolyte. Assembly drawing of the Li–O₂ coin battery; mechanical strength measurements of the membranes; physicochemical properties of the Janus membrane-based GPE; electrochemical reversibility of the Li–O₂ batteries; galvanostatic discharge profiles of Li–O₂ battery without the cathode at 100 mA g⁻¹; TEM image of δ-MnO₂@CNTs as the contrastive cathode; SEM image of the air cathode initially discharged with

LiTFSI-based liquid electrolyte; FTIR spectra and XRD pattern of the discharge product on air cathode and near the membrane (PDF)

■ AUTHOR INFORMATION

Corresponding Author

*E-mail: lianfang@mater.ustb.edu.cn. Tel: +86 10 82377985.

Fax: +86 10 82377985.

ORCID

Fang Lian: 0000-0002-6446-4432

Hong Li: 0000-0002-8659-086X

Notes

The authors declare no competing financial interest.

■ ACKNOWLEDGMENTS

This work was supported by Beijing Municipal Science and Technology Project (Nos. D151100003115002 and Z181100004518003) and Fundamental Research Funds for the Central Universities (No. FRF-GF-17-B10).

■ REFERENCES

- (1) Abraham, K. M.; Jiang, Z. A polymer electrolyte-based rechargeable lithium/oxygen battery. *J. Electrochem. Soc.* **1996**, *143*, 1–5.
- (2) Ogasawara, T.; Debart, A.; Holzapfel, M.; Novak, P.; Bruce, P. G. Rechargeable Li₂O₂ electrode for lithium batteries. *J. Am. Chem. Soc.* **2006**, *128*, 1390–1393.
- (3) Bruce, P. G.; Freunberger, S. A.; Hardwick, L. J.; Tarascon, J.-M. Li–O₂ and Li–S batteries with high energy storage. *Nat. Mater.* **2011**, *11*, 19–29.
- (4) Girishkumar, G.; McCloskey, B.; Luntz, A. C.; Swanson, S.; Wilcke, W. Lithium–Air Battery: Promise and Challenges. *J. Phys. Chem. Lett.* **2010**, *1*, 2193–2203.
- (5) Imanishi, N.; Luntz, A. C.; Bruce, P. G. *The Lithium Air Battery: Fundamentals*; Springer: New York, 2014.
- (6) Freunberger, S. A.; Chen, Y.; Peng, Z.; et al. Reactions in the rechargeable Li–O₂ battery with alkyl carbonate electrolytes. *J. Am. Chem. Soc.* **2011**, *133*, 8040–8047.
- (7) Tokur, M.; Algul, H.; Cetinkaya, T.; Uysal, M.; Akbulut, H. Improved Electrochemical Performance of Lithium Oxygen Batteries with N-methyl-2-pyrrolidone Based Composite Polymer Electrolytes. *J. Electrochem. Soc.* **2016**, *163*, A1326–A1335.
- (8) Yi, J.; Liu, X.; Guo, S.; Zhu, K.; Xue, H.; Zhou, H. Novel Stable Gel Polymer Electrolyte: Toward a High Safety and Long Life Li–Air Battery. *ACS Appl. Mater. Interfaces* **2015**, *7*, 23798–23804.
- (9) Elia, G. A.; Hassoun, J. A gel polymer membrane for lithium-ion oxygen battery. *Solid State Ionics* **2016**, *287*, 22–27.
- (10) Liu, T.; Chang, Z.; Yin, Y.; Chen, K.; Zhang, Y.; Zhang, X. The PVDF-HFP gel polymer electrolyte for Li–O₂ battery. *Solid State Ionics* **2018**, *318*, 88–94.
- (11) Zhu, Y.; Wang, F.; Liu, L.; Xiao, S.; Chang, Z.; Wu, Y. Composite of a nonwoven fabric with poly(vinylidene fluoride) as a gel membrane of high safety for lithium ion battery. *Energy Environ. Sci.* **2013**, *6*, 618–624.
- (12) Zhu, Y.; Xiao, S.; Shi, Y.; Yang, Y.; Wu, Y. A trilayer poly(vinylidene fluoride)/polyborate/poly(vinylidene fluoride) gel polymer electrolyte with good performance for lithium ion batteries. *J. Mater. Chem. A* **2013**, *1*, 7790–7797.
- (13) Zhu, Y.; Wang, F.; Liu, L.; Xiao, S.; Yang, Y.; Wu, Y. Cheap glass fiber mats as a matrix of gel polymer electrolytes for lithium ion batteries. *Sci. Rep.* **2013**, *3*, No. 3187.
- (14) Zhu, Y.; Xiao, S.; Shi, Y.; Yang, Y.; Hou, Y.; Wu, Y. A Composite Gel Polymer Electrolyte with High Performance Based on Poly(Vinylidene Fluoride) and Polyborate for Lithium Ion Batteries. *Adv. Energy Mater.* **2014**, *4*, No. 1300647.

- (15) Wang, J.; Yin, Y.; Liu, T.; Yang, X.; Chang, Z.; Zhang, X. Hybrid electrolyte with robust garnet-ceramic electrolyte for lithium anode protection in lithium-oxygen batteries. *Nano Res.* **2018**, *3434–3441*.
- (16) Xu, J.-J.; Liu, Q.-C.; Yu, Y.; Wang, J.; Yan, J.-M.; Zhang, X.-B. In Situ Construction of Stable Tissue-Directed/Reinforced Bifunctional Separator/Protection Film on Lithium Anode for Lithium-Oxygen Batteries. *Adv. Mater.* **2017**, *29*, No. 1606552.
- (17) Liu, Q.; Chang, Z.; Li, Z.; Zhang, X. Flexible metal-air batteries: progress, challenges, and perspectives. *Small Methods* **2018**, *2*, No. 1700231.
- (18) Yang, X.-y.; Xu, J.-j.; Bao, D.; Chang, Z.-w.; Liu, D.-p.; Zhang, Y.; Zhang, X.-B. High-Performance Integrated Self-Package Flexible Li-O₂ Battery Based on Stable Composite Anode and Flexible Gas Diffusion Layer. *Adv. Mater.* **2017**, *29*, No. 1700378.
- (19) Liu, T.; Xu, J.-J.; Liu, Q.-C.; Chang, Z.-W.; Yin, Y.-B.; Yang, X.-Y.; Zhang, X.-B. Ultrathin, Lightweight, and Wearable Li-O₂ Battery with High Robustness and Gravimetric/Volumetric Energy Density. *Small* **2017**, *13*, No. 1602952.
- (20) Yi, J.; Guo, S.; He, P.; Zhou, H. Status and prospects of polymer electrolytes for solid-state Li-O₂ (air) batteries. *Energy Environ. Sci.* **2017**, *10*, 860–884.
- (21) Lian, F.; Wen, Y.; Ren, Y.; Guan, H. A novel PVB based polymer membrane and its application in gel polymer electrolytes for lithium-ion batteries. *J. Membr. Sci.* **2014**, *456*, 42–48.
- (22) Guan, H.-y.; Lian, F.; Xi, K.; Ren, Y.; Sun, J.-L.; Kumar, R. V. Polyvinyl formal based gel polymer electrolyte prepared using initiator free in-situ thermal polymerization method. *J. Power Sources* **2014**, *245*, 95–100.
- (23) Ren, Y.; Lian, F.; Wen, Y.; Guan, H.-Y. A novel PVFM based membranes prepared via phase inversion method and its application in GPE. *Polymer* **2013**, *54*, 4807–4813.
- (24) Li, Y.; Wang, X.; Dong, S.; Chen, X.; Cui, G. Recent Advances in nonAqueous Electrolyte for Rechargeable Li-O₂ Batteries. *Adv. Energy Mater.* **2016**, *6*, No. 1600751.
- (25) Wen, Y.; Lian, F.; Ren, Y.; Guan, H.-Y. Enhanced Electrochemical Properties of a Novel Polyvinyl Formal Membrane Supporting Gel Polymer Electrolyte by Al₂O₃ Modification. *J. Polym. Sci., Part B: Polym. Phys.* **2014**, *52*, 572–577.
- (26) Kuboki, T.; Okuyama, T.; Ohsaki, T.; Takami, N. Lithium-air batteries using hydrophobic room temperature ionic liquid electrolyte. *J. Power Sources* **2005**, *146*, 766–769.
- (27) Soavi, F.; Monaco, S.; Mastragostino, M. Catalyst-free porous carbon cathode and ionic liquid for high efficiency, rechargeable Li/O₂ battery. *J. Power Sources* **2013**, *224*, 115–119.
- (28) Elia, G. A.; Hassoun, J.; Kwak, W. J.; Sun, Y. K.; Scrosati, B.; Mueller, F.; Bresser, D.; Passerini, S.; Oberhumer, P.; Tsiouvaras, N.; Reiter, J. An Advanced Lithium-Air Battery Exploiting an Ionic Liquid-Based Electrolyte. *Nano Lett.* **2014**, *14*, 6572–6577.
- (29) Wu, C.; Liao, C.; Li, T.; Shi, Y.; Luo, J.; Li, L.; Yang, J. A polymer lithium-oxygen battery based on semi-polymeric conducting ionomers as the polymer electrolyte. *J. Mater. Chem. A* **2016**, *4*, 15189–15196.
- (30) Peng, Z.; Freunberger, S. A.; Chen, Y.; Bruce, P. G. A Reversible and Higher-Rate Li-O₂ Battery. *Science* **2012**, *337*, 563–566.
- (31) Marinaro, M.; Theil, S.; Joerissen, L.; Wohlfahrt-Mehrens, M. New insights about the stability of lithium bis(trifluoromethane)-sulfonamide-tetraglyme as electrolyte for Li-O₂ batteries. *Electrochim. Acta* **2013**, *108*, 795–800.
- (32) Lu, J.; Lee, Y. J.; Luo, X.; Lau, K. C.; Asadi, M.; Wang, H.-H.; Brombosz, S.; Wen, J.; Zhai, D.; Chen, Z.; Miller, D. J.; Jeong, Y. S.; Park, J.-B.; Fang, Z. Z.; Kumar, B.; Salehi-Khojin, A.; Sun, Y.-K.; Curtiss, L. A.; Amine, K. A lithium-oxygen battery based on lithium superoxide. *Nature* **2016**, *529*, 377.
- (33) Zhang, J.; Sun, B.; Xie, X.; Kretschmer, K.; Wang, G. Enhancement of stability for lithium oxygen batteries by employing electrolytes gelled by poly(vinylidene fluoride-co-hexafluoropropylene) and tetraethylene glycol dimethyl ether. *Electrochim. Acta* **2015**, *183*, 56–62.
- (34) Chou, K.-C.; Zhong, X. M.; Xu, K. D. Calculation of physicochemical properties in a ternary system with miscibility gap. *Metall. Mater. Trans. B* **2004**, *35*, 715–720.
- (35) Zhang, S. S.; Ervin, M. H.; Xu, K.; Jow, T. R. Microporous poly(acrylonitrile-methyl methacrylate) membrane as a separator of rechargeable lithium battery. *Electrochim. Acta* **2004**, *49*, 3339–3345.
- (36) Elia, G. A.; Hassoun, J. A Polymer Lithium-Oxygen Battery. *Sci. Rep.* **2015**, *5*, No. 12307.
- (37) Aurbach, D. Review of selected electrode-solution interactions which determine the performance of Li and Li ion batteries. *J. Power Sources* **2000**, *89*, 206–218.
- (38) Zhang, D.; Li, R.; Huang, T.; Yu, A. Novel composite polymer electrolyte for lithium air batteries. *J. Power Sources* **2010**, *195*, 1202–1206.
- (39) Wu, S.; Yi, J.; Zhu, K.; Bai, S.; Liu, Y.; Qiao, Y.; Ishida, M.; Zhou, H. A Super-Hydrophobic Quasi-Solid Electrolyte for Li-O₂ Battery with Improved Safety and Cycle Life in Humid Atmosphere. *Adv. Energy Mater.* **2017**, *7*, No. 1601759.
- (40) Tong, B.; Huang, J.; Zhou, Z.; Peng, Z. The Salt Matters: Enhanced Reversibility of Li-O₂ Batteries with a Li (CF₃SO₂)(n-C₄F₉SO₂)N -Based Electrolyte. *Adv. Mater.* **2018**, *30*, No. 1704841.
- (41) Guo, Z.; Li, C.; Liu, J.; Wang, Y.; Xia, Y. A Long-Life Lithium-Air Battery in Ambient Air with a Polymer Electrolyte Containing a Redox Mediator. *Angew. Chem., Int. Ed.* **2017**, *56*, 7505–7509.
- (42) Liu, T.; Liu, Q.-C.; Xu, J.-J.; Zhang, X.-B. Cable-Type Water-Survivable Flexible Li-O₂ Battery. *Small* **2016**, *12*, 3101–3105.
- (43) Leng, L.; Zeng, X.; Chen, P.; Shu, T.; Song, H.; Fu, Z.; Wang, H.; Liao, S. A novel stability-enhanced lithium-oxygen battery with cellulose-based composite polymer gel as the electrolyte. *Electrochim. Acta* **2015**, *176*, 1108–1115.
- (44) Chung, S.-H.; Han, P.; Singhal, R.; Kalra, V.; Manthiram, A. Electrochemically Stable Rechargeable Lithium-Sulfur Batteries with a Microporous Carbon Nanofiber Filter for Polysulfide. *Adv. Energy Mater.* **2015**, *5*, No. 1500738.
- (45) Chamaani, A.; Safa, M.; Chawla, N.; El-Zahab, B. Composite Gel Polymer Electrolyte for Improved Cyclability in Lithium-Oxygen Batteries. *ACS Appl. Mater. Interfaces* **2017**, *9*, 33819–33826.
- (46) Chung, S.-H.; Manthiram, A. A Polyethylene Glycol-Supported Microporous Carbon Coating as a Polysulfide Trap for Utilizing Pure Sulfur Cathodes in Lithium-Sulfur Batteries. *Adv. Mater.* **2014**, *26*, 7352–7357.
- (47) Lee, S. H.; Park, J.-B.; Lim, H.-S.; Sun, Y.-K. An Advanced Separator for Li-O₂ Batteries: Maximizing the Effect of Redox Mediators. *Adv. Energy Mater.* **2017**, *7*, No. 1602417.
- (48) Yi, J.; Zhou, H. A Unique Hybrid Quasi-Solid-State Electrolyte for Li-O₂ Batteries with Improved Cycle Life and Safety. *ChemSusChem* **2016**, *9*, 2391–2396.
- (49) Chamaani, A.; Chawla, N.; Safa, M.; El-Zahab, B. One-Dimensional Glass Micro-Fillers in Gel Polymer Electrolytes for Li-O₂ Battery Applications. *Electrochim. Acta* **2017**, *235*, 56–63.
- (50) Liu, Q.-C.; Liu, T.; Liu, D.-P.; Li, Z.-J.; Zhang, X.-B.; Zhang, Y. A Flexible and Wearable Lithium-Oxygen Battery with Record Energy Density achieved by the Interlaced Architecture inspired by Bamboo Slips. *Adv. Mater.* **2016**, *28*, 8413–8418.
- (51) Kim, Y. B.; Kim, I. T.; Song, M. J.; Shin, M. W. Poly(vinylidene-fluoride)-ip-benzoquinone gel polymer electrolyte with good performance by redox mediator effect for Li-air battery. *Electrochim. Acta* **2016**, *210*, 821–828.
- (52) Liu, S.; Zhu, Y.; Xie, J.; Huo, Y.; Yang, H. Y.; Zhu, T.; Cao, G.; Zhao, X.; Zhang, S. Direct Growth of Flower-Like δ-MnO₂ on Three-Dimensional Graphene for High-Performance Rechargeable Li-O₂ Batteries. *Adv. Energy Mater.* **2014**, *4*, No. 1301960.
- (53) Ozcan, S.; Tokur, M.; Cetinkaya, T.; Guler, A.; Uysal, M.; Guler, M. O.; Akbulut, H. Free standing flexible graphene oxide plus α-MnO₂ composite cathodes for Li-Air batteries. *Solid State Ionics* **2016**, *286*, 34–39.

(54) Kavakli, C.; Meini, S.; Harzer, G.; Tsiouvaras, N.; Piana, M.; Siebel, A.; Garsuch, A.; Gasteiger, H. A.; Herranz, J. Nanosized Carbon-Supported Manganese Oxide Phases as Lithium-Oxygen Battery Cathode Catalysts. *ChemCatChem* **2013**, *5*, 3358–3373.

(55) Togasaki, N.; Gohara, T.; Momma, T.; Osaka, T.; Numata, T. A Comparative Study of LiNO₃ and LiTFSI for the Cycling Performance of δ -MnO₂ Cathode in Lithium-Oxygen Batteries. *J. Electrochem. Soc.* **2017**, *164*, A2225–A2230.

(56) Yoon, K. R.; Shin, K.; Park, J.; Cho, S.-H.; Kim, C.; Jung, J.-W.; Cheong, J. Y.; Byon, H. R.; Lee, H. M.; Kim, I.-D. Brush-Like Cobalt Nitride Anchored Carbon Nanofiber Membrane: Current Collector Catalyst Integrated Cathode for Long Cycle Li-O₂ Batteries. *ACS Nano* **2018**, *12*, 128–139.

(57) Zhang, S.; Wang, G.; Jin, J.; Zhang, L.; Wen, Z.; Yang, J. Self-catalyzed decomposition of discharge products on the oxygen vacancy sites of MoO₃ nanosheets for low-overpotential Li-O₂ batteries. *Nano Energy* **2017**, *36*, 186–196.

(58) Eftekhari, A.; Ramanujam, B. In pursuit of catalytic cathodes for lithium-oxygen batteries. *J. Mater. Chem. A* **2017**, *5*, 7710–7731.

(59) Zheng, H.; Xiao, D.; Li, X.; Liu, Y.; Wu, Y.; Wang, J.; Jiang, K.; Chen, C.; Gu, L.; Wei, X.; Hu, Y.-S.; Chen, Q.; Li, H. New Insight in Understanding Oxygen Reduction and Evolution in Solid-State Lithium Oxygen Batteries Using an in Situ Environmental Scanning Electron Microscope. *Nano Lett.* **2014**, *14*, 4245–4249.